

Nucleosynthesis and abundances of light elements

Big Bang nucleosynthesis (BBNS)

very successful, in particular

- primordial abundances of light elements
 ^2D , ^3He , ^4He , ^7Li

- number of ν 's $H\nu < 4$

1990 τ_0 decay width measured at CERN
 $H\nu \leq 3$

- neutron half-life time

BB theory: $\tau \leq 10.4 \text{ min}$, today $\tau = 10.28 \text{ min}$

temperature decreases as Universe expands

$$T_\gamma = 0,96 \cdot 10^{10} t^{-\frac{1}{2}} \text{ K}$$

$$\text{or } hT = 0,8 t^{-\frac{1}{2}} \text{ MeV}$$

elements are synthesized 3 min after BB

\Rightarrow more, see lecture: Newtonian Cosmology

neutron-proton ratio

before γe decoupling at 1 MeV

thermal equilibrium of p & n



History of the Universe

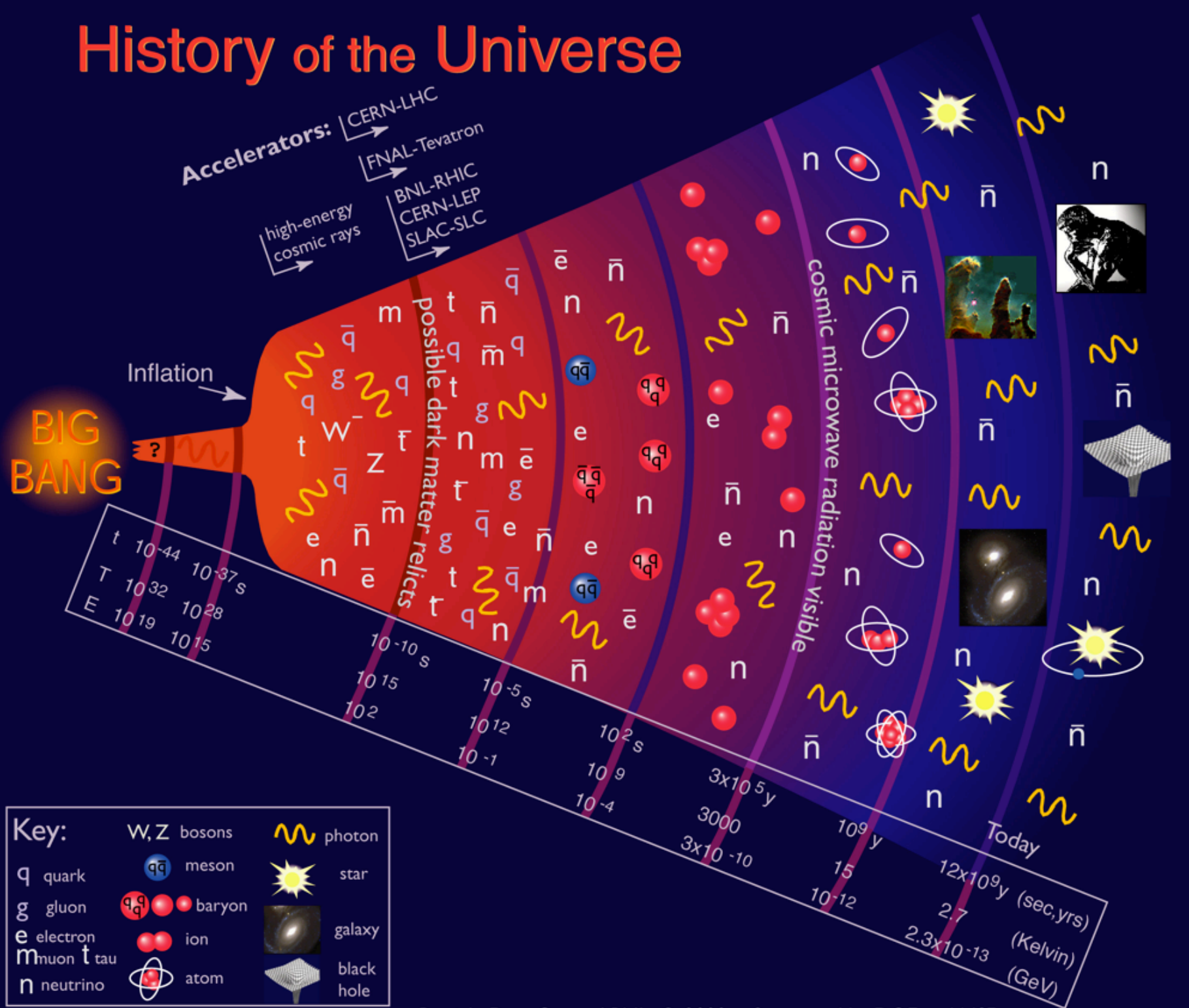


Table 4.1. Brief thermal history of the Universe

	Time	kT_γ	T_γ	g_*	
Un-certain physics	10^{-42} s	10^{19} GeV			Planck era; quantum grav.
	10^{-35} s	10^{15} GeV			GUTs, Infl., Primord. fluct.
	10^{-9} s	100 GeV		~ 100	Electroweak trans.
	10^{-4} s	150 MeV		20	Q-H trans.; meson decay
Physics fairly well known	1 s	1 MeV	10^{10} K	43/4	Weak interaction decoupl.; e^\pm annihilation; $T_\nu < T_\gamma$
	100 s	0.1 MeV	10^9 K	3.36	BBNS (D, ${}^3\text{He}$, ${}^4\text{He}$, ${}^7\text{Li}$)
					Matter domination
Un-certain details	4×10^5 yr	0.2 eV	3000 K		(Re)comb.; MWB last scat.
	10^8 yr	4×10^{-3} eV	50 K		Re-ionization;
	10^{10} yr	2×10^{-4} eV	3 K		Structure formation Present

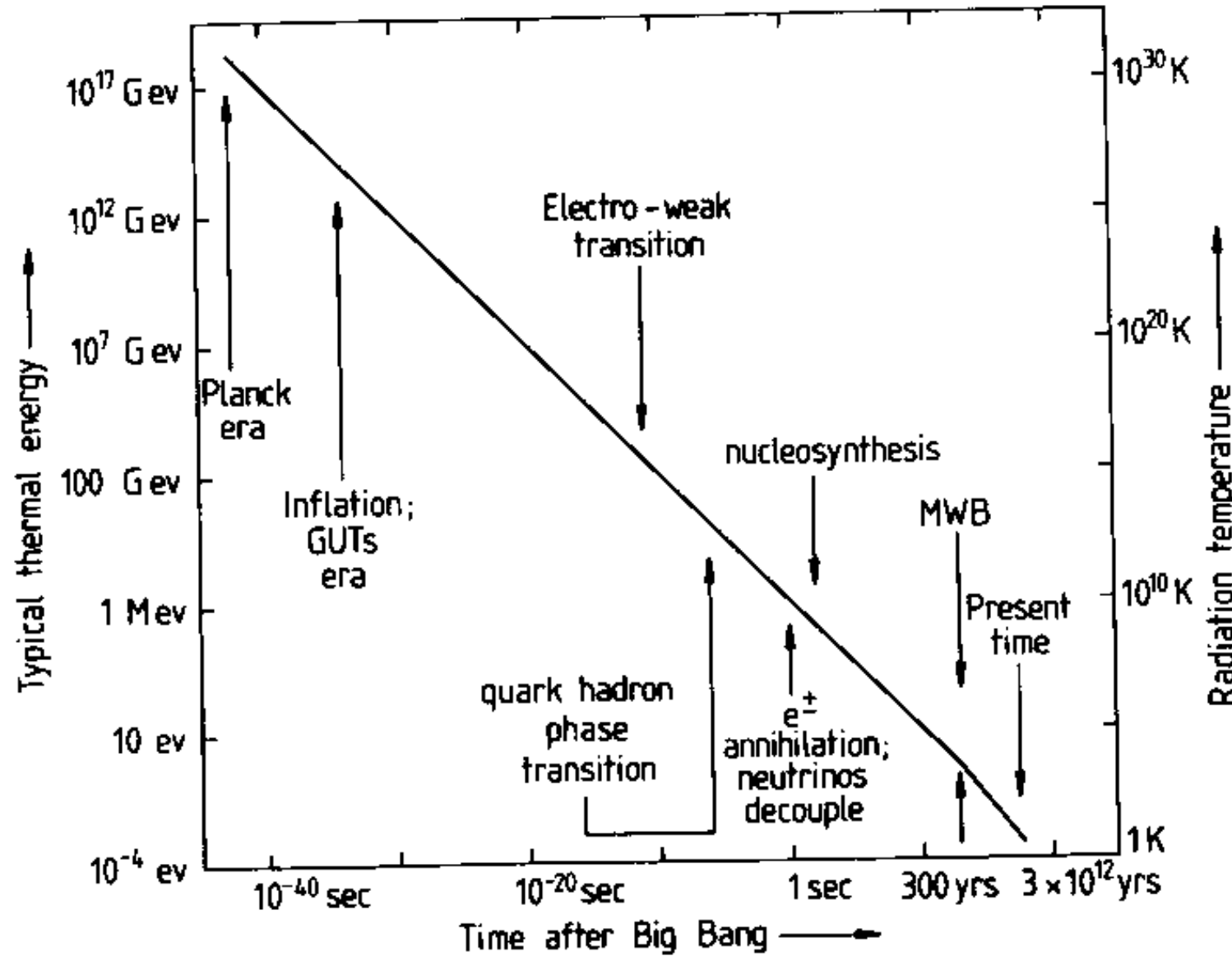
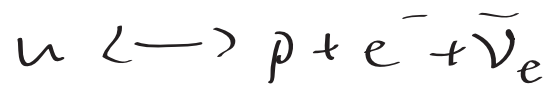
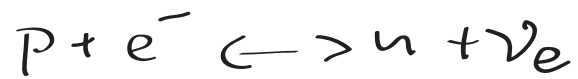


Fig. 4.1. Schematic thermal history of the Universe showing some of the major episodes envisaged in the standard model. GUTs is short for grand unification theories and MWB is short for (the last scattering of) the microwave background radiation. The Universe is dominated by radiation and relativistic particles up to a time a little before that of MWB and by matter (including non-baryonic matter) thereafter, with dark energy eventually taking over.



chemical potentials of p & n are equal

\rightarrow Boltzmann type equilibrium ratio

$$\left(\frac{n}{p}\right)_{eq} = e^{-\frac{(m_n - m_p)c^2}{kT}} = e^{-1.29 \text{ MeV}/kT}$$

at temperature $kT_d = 0.8 \text{ MeV}$ weak interaction

rate falls suddenly below the expansion rate

and $\frac{n}{p}$ is frozen

$$\frac{n}{p} = e^{-1.29 \text{ MeV}/kT_d} \approx 0.2$$

→ primordial helium mass fraction Y_p
all neutrons snatched up to make ^4He

$$Y_p = \frac{2n}{n+p} \approx 0.25 \quad \text{after free decay for about 200 s}$$

decoupling temperature T_d

$$T_d^2 \propto T_{\frac{1}{2}}^2 \left(\frac{11}{4} + \frac{7}{8} N_\nu \right)^{\frac{1}{2}}$$

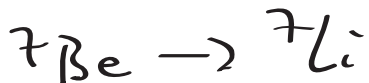
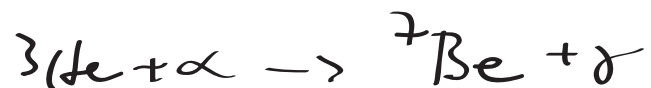
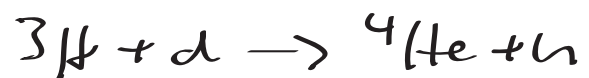
$\tau_{\frac{1}{2}}$ neutrino half lifetime
 N_ν # of ν generations

↑

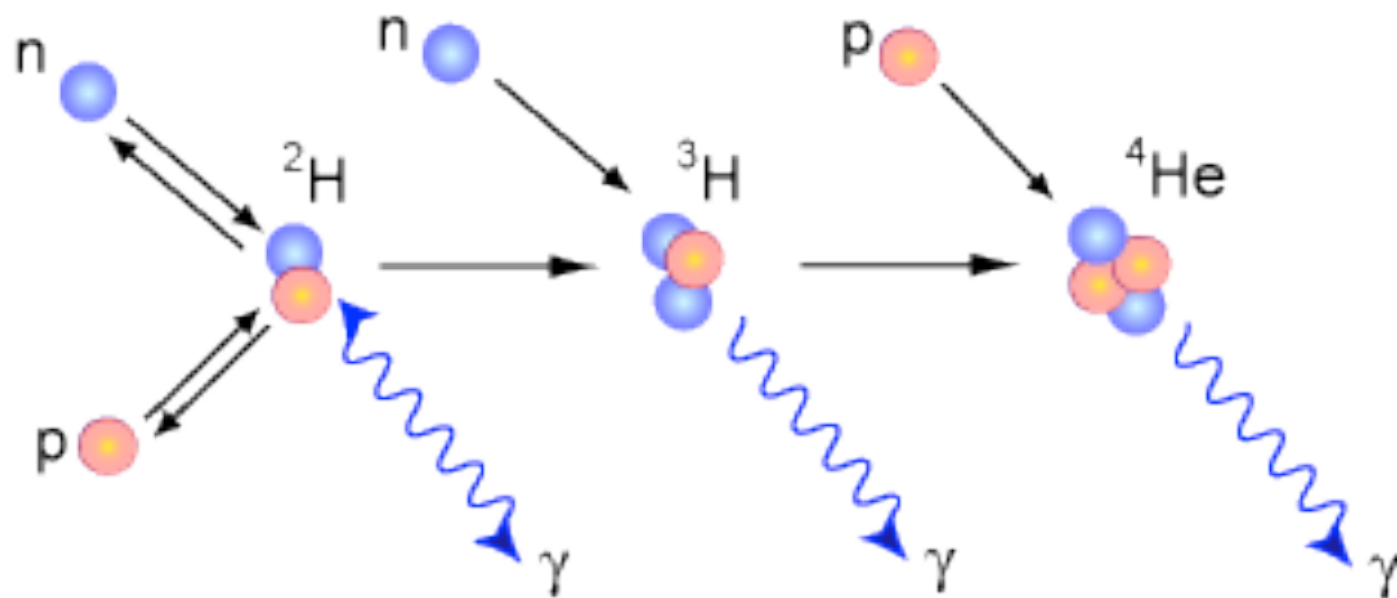
from effective number of degrees of freedom

nuclear reactions

primordial nucleosynthesis is mainly due to



Big Bang Nucleosynthesis



This shows one of the reaction sequences that produces a helium-4 nucleus from protons and neutrons. Other sequences are possible. The first stage is reversible due to photodisintegration by gamma photons.

at $kT \approx 0.3 \text{ MeV}$ $\Upsilon_p \approx 0.15$ (for $\frac{u}{p} \approx 0.2$)

nuclear reactions become slow

(Coulomb barriers & low abundances of $D, {}^3\text{H}, {}^3\text{He}$)

at $kT = 0.1 \text{ MeV}$ $\frac{d}{P} \approx 10^{-5}$

nuclear reactions effectively build up to ${}^4\text{He}$

after formation of ${}^4\text{He}$, traces of lighter elements

survive because nuclear reactions are frozen out
by low temperatures & density

small fractions of ${}^7\text{Li} + {}^7\text{Be}$ remain

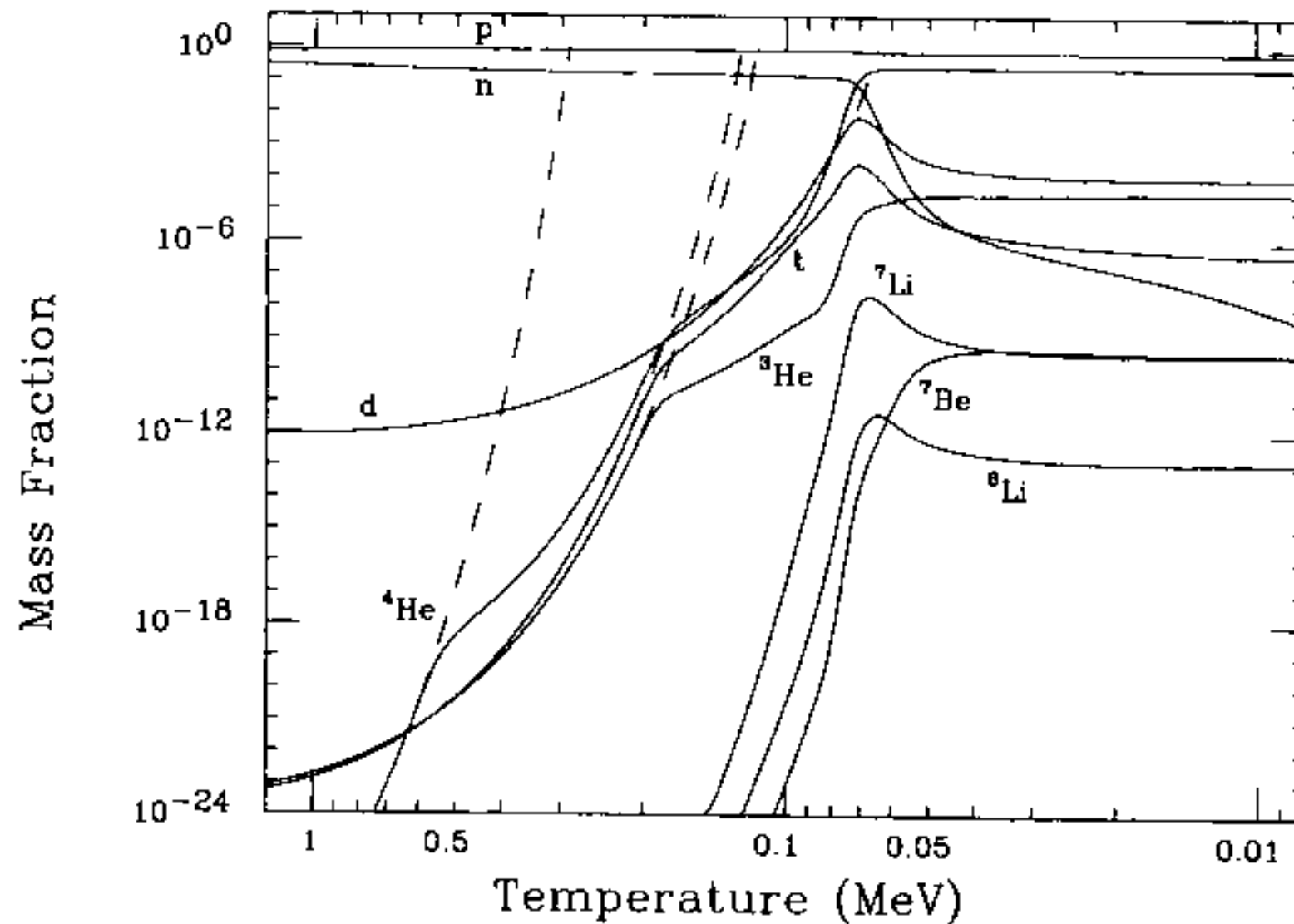


Fig. 4.2. Evolution of light-element abundances with temperature, for $\eta_{10} = 3.16$. The dashed curves give the nuclear statistical equilibrium abundances for ${}^4\text{He}$, ${}^3\text{He}$, ${}^3\text{H}(t)$ and ${}^2\text{D}(d)$ respectively; the dotted curve for ${}^2\text{D}$ allows for the diminishing number of free neutrons. After Smith, Kawano and Malaney (1993). Courtesy Michael Smith.

baryon-photon ratio $\eta = \frac{n_b}{n_\gamma} = \text{const.} \simeq 10^{-10} \text{ to } 10^{-9}$

abundance of elements depends on η

- ^4He not very sensitive to η
- D easily destroyed \rightarrow strong dependence on η
 ^3He more robust
- ^7Li at low η synthesized $^3\text{H} + \alpha \rightarrow ^7\text{Li} + \gamma$
high η $^3\text{He} + \alpha \rightarrow ^7\text{Be} + \gamma$ $^7\text{Be} \rightarrow ^7\text{Li}$

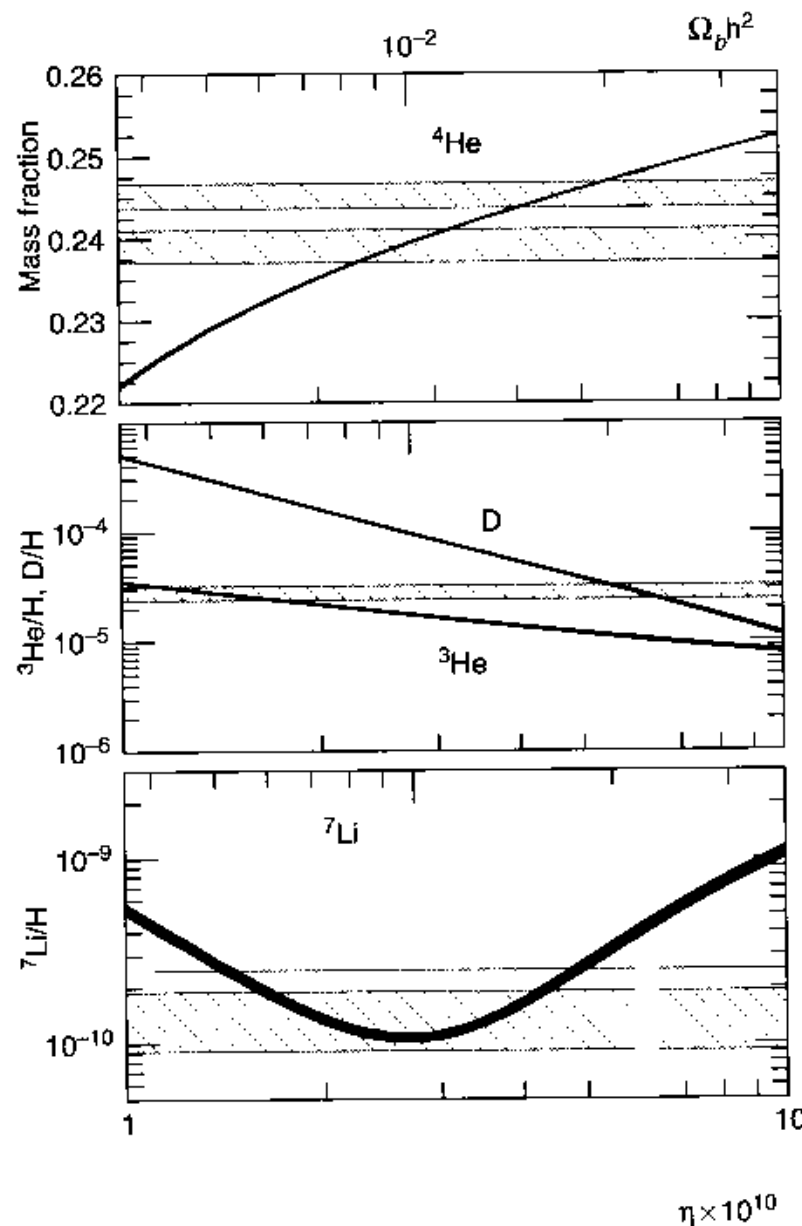
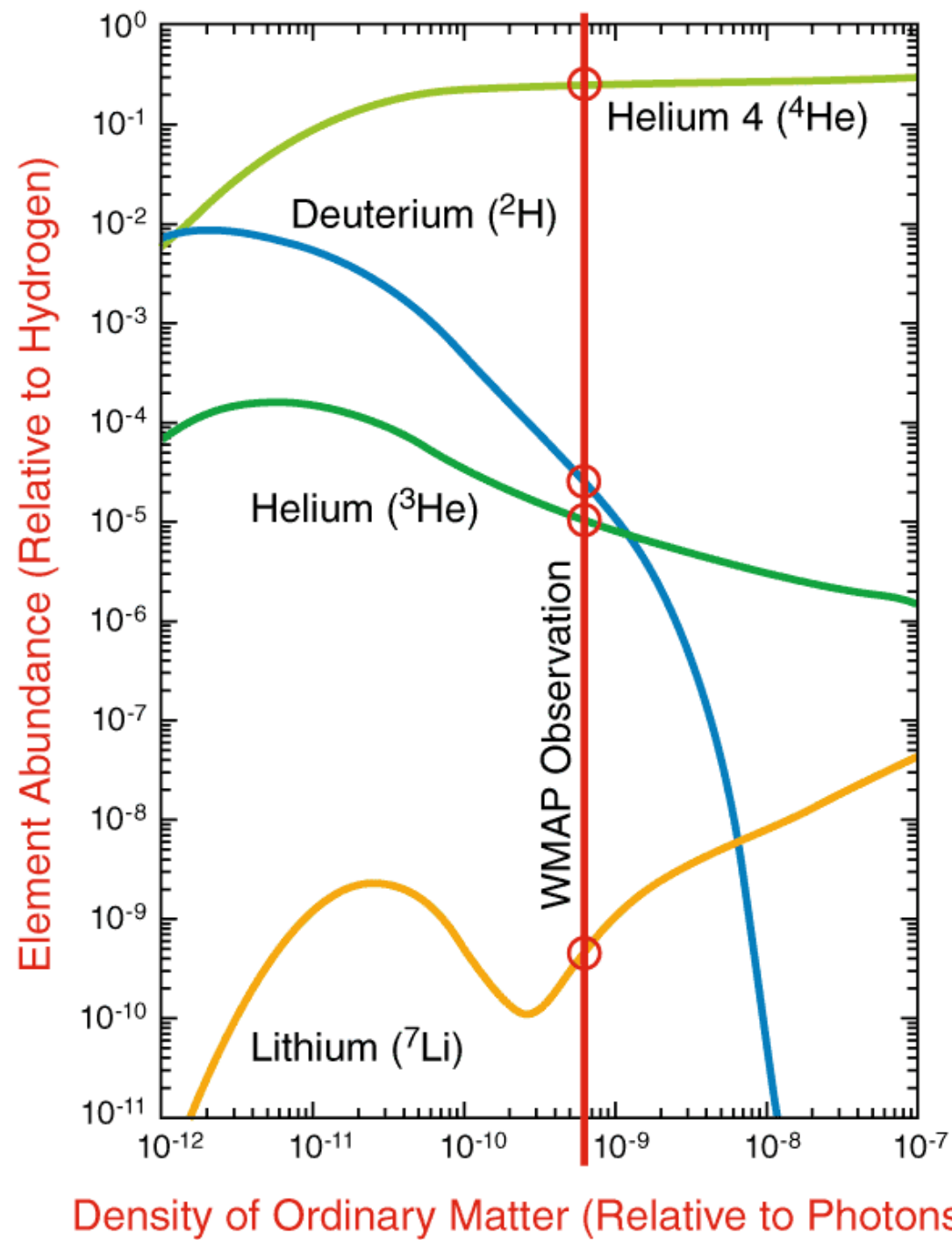


Fig. 4.3. Primordial abundances from SBBN as functions of η or, equivalently, $\Omega_{b0}h^2$. Curves show theoretical predictions, with their $\pm 1\sigma$ uncertainty limits represented by the thickness of the curves, while the horizontal error boxes indicate various limits derived from observation. (Observational estimates of ${}^4\text{He}$ have since been revised upwards.) The vertical bar indicates the range of η deduced from WMAP observations of the angular fluctuation power spectrum of the MWB (Spergel *et al.* 2003). After Coc *et al.* (2004).



Dendrium & ^3He

all D in Universe is from BBNs

thermonuclear reactions in stars \rightarrow destruction of D

$\frac{D}{H} \sim 2,0 \cdot 10^{-5}$ from observations of HD & CH_3D

in atmospheres of major planets

interstellar ratio $\frac{D}{H} \sim 1,5 \cdot 10^{-5}$

absorption lines of H due to gas along the

line of sight to quasars at high redshift $\rightarrow \frac{D}{H}$

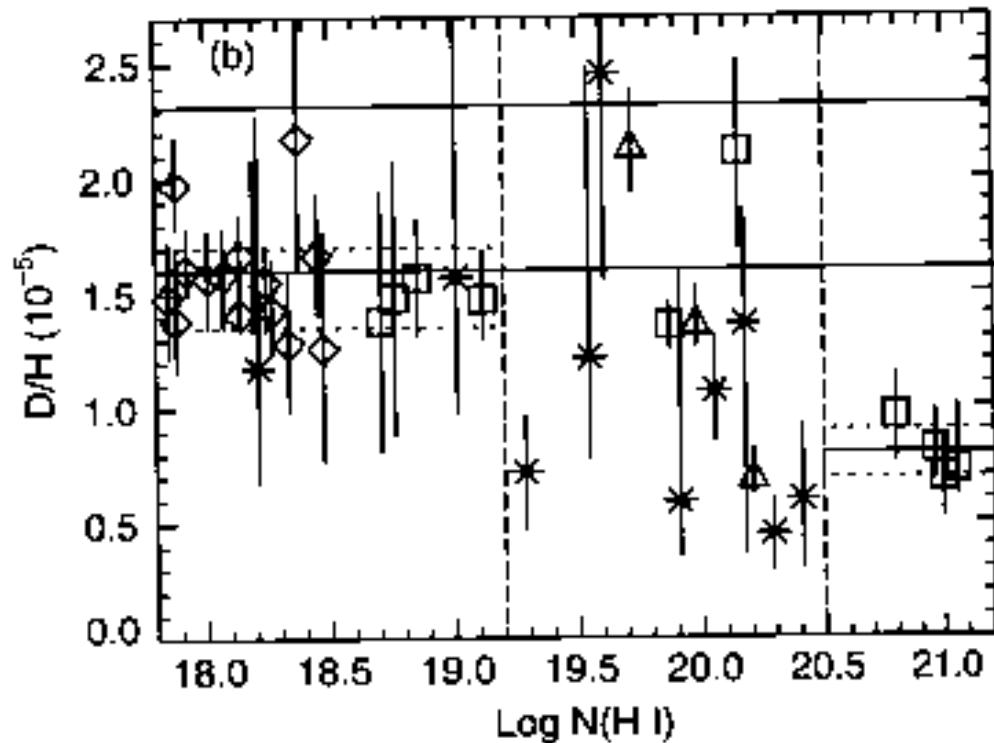
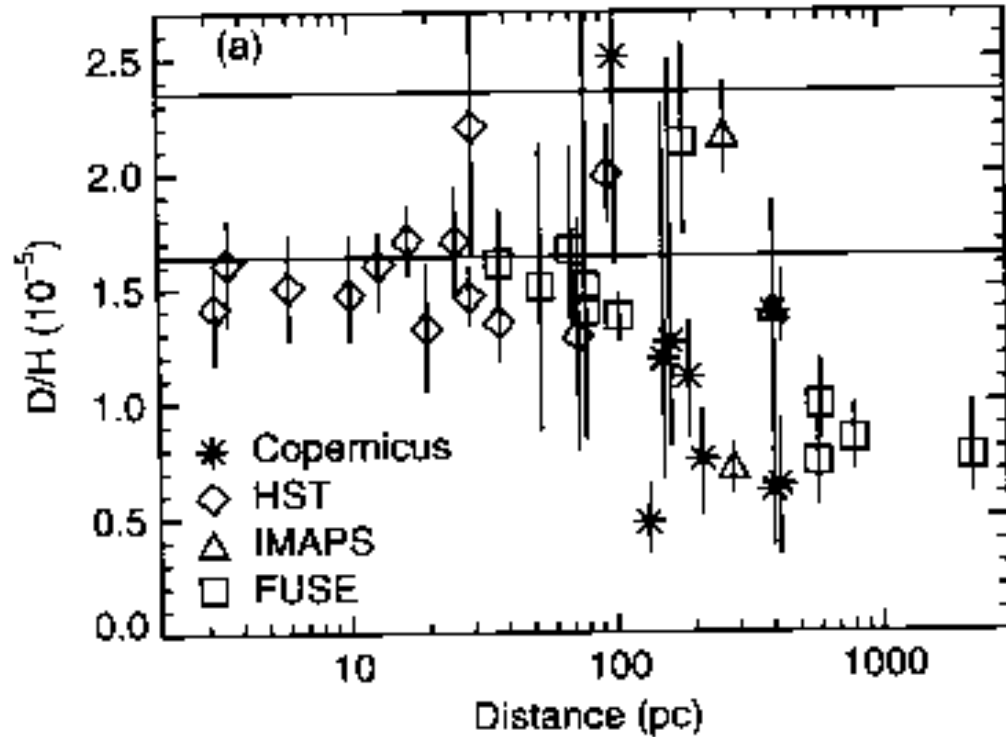


Fig. 4.4. D/H ratios measured along the lines of sight to stars in the Galaxy. The horizontal parallel lines indicate upper and lower limits to the ratio in the protosolar cloud after Geiss and Gloeckler (2003). Adapted from Wood *et al.* (2004).

clear samples:

$$4,5 \leq \gamma_{10} \leq 7 \quad \text{or} \quad 0,015 \leq \Omega_{b_0} h^2 \leq 0,025$$

$$h = 0,7 \quad 0,03 \leq \Omega_{b_0} \leq 0,05$$

^3He detected in galactic H II regions with radio telescopes

hyperfine transition of $^3\text{He}^+$

Helium

primordial Υ_p difficult ^4He is synthesized in stars

$0,23 \leq \Upsilon_p \leq 0,25$ generally accepted

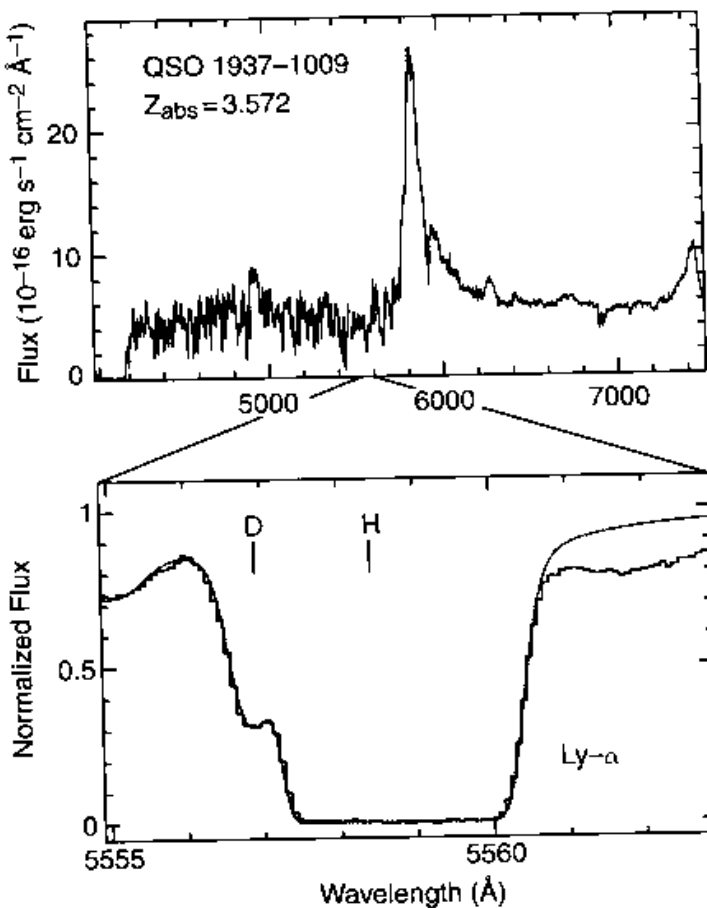


Fig. 4.5. Determination of the D/H ratio in an intervening (Lyman-limit) absorption-line system in front of the quasar 1937-1009. The upper panel shows Lyman- α and a few other emission lines from the quasar, while shortward of Lyman- α there is a multitude of Lyman- α absorption lines (the ‘Lyman- α forest’) from density fluctuations in the intergalactic medium, with one cloud having sufficient column density to produce strong absorption at the Lyman limit, redshifted to 4200 Å. The factor 100 drop in the continuum at that point (measured on spectra with higher signal:noise) gives the hydrogen column density. The lower panel shows a high-resolution spectrum of the Lyman- α line from the same system in which the deuterium component clearly appears and enables the deuterium column density to be determined, giving $D/H = (3.3 \pm 0.3) \times 10^{-5}$. This is one of a mere handful of known systems deemed to be ‘clean’, i.e. free from contamination by hydrogen moving at around 82 km s^{-1} towards us relative to the main component. Reprinted from Tytler, O’Meara, Suzuki and Lubin (2000). With permission from Elsevier.

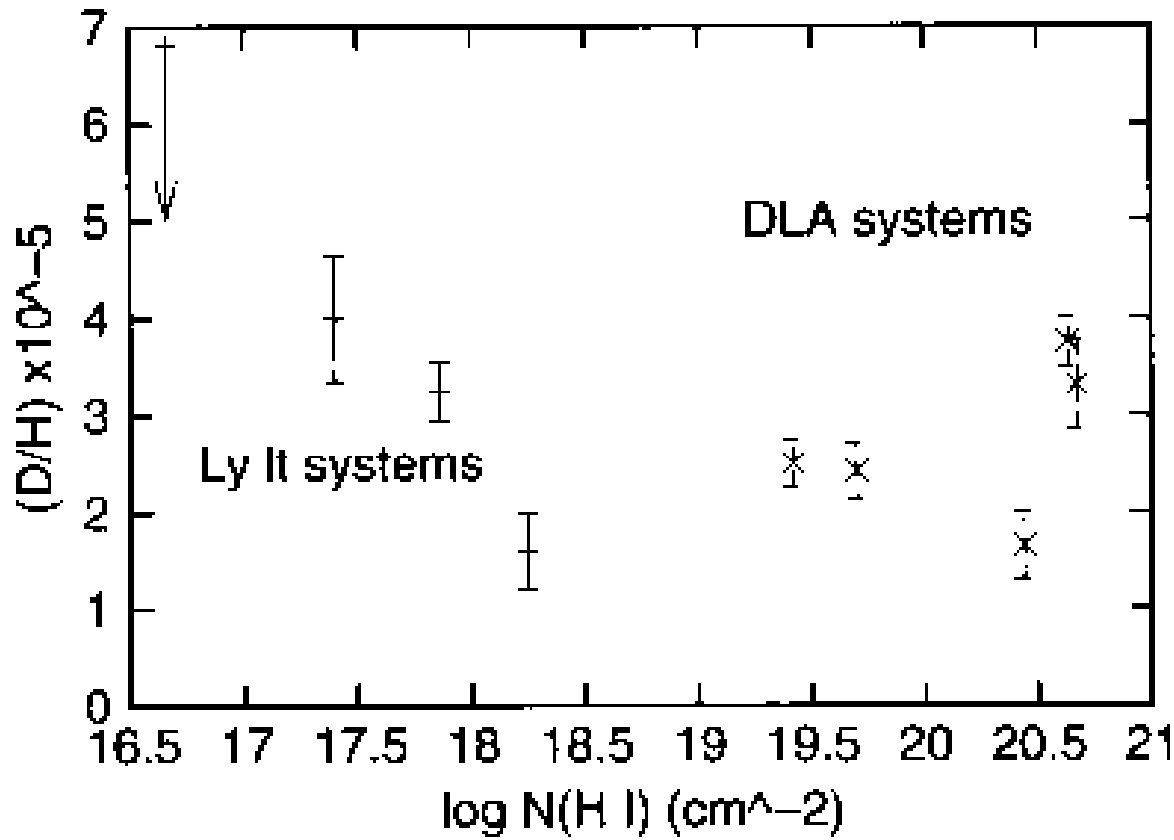


Fig. 4.6. Comparison of D/H measurements at high redshift from Lyman-limit and damped Lyman- α systems. The measurements come from O'Meara *et al.* (2001; 3 Lyman-limit systems and one marginal DLA), Crighton *et al.* (2004; the highest column density Lyman-limit system), Kirkman *et al.* (2003; another marginal DLA), Pettini & Bowen (2001), Levshakov *et al.* (2002) and O'Meara *et al.* (2006) (three classical DLAs). There is no convincing evidence for systematic trends with either column density or metallicity up to about 1/30 solar.

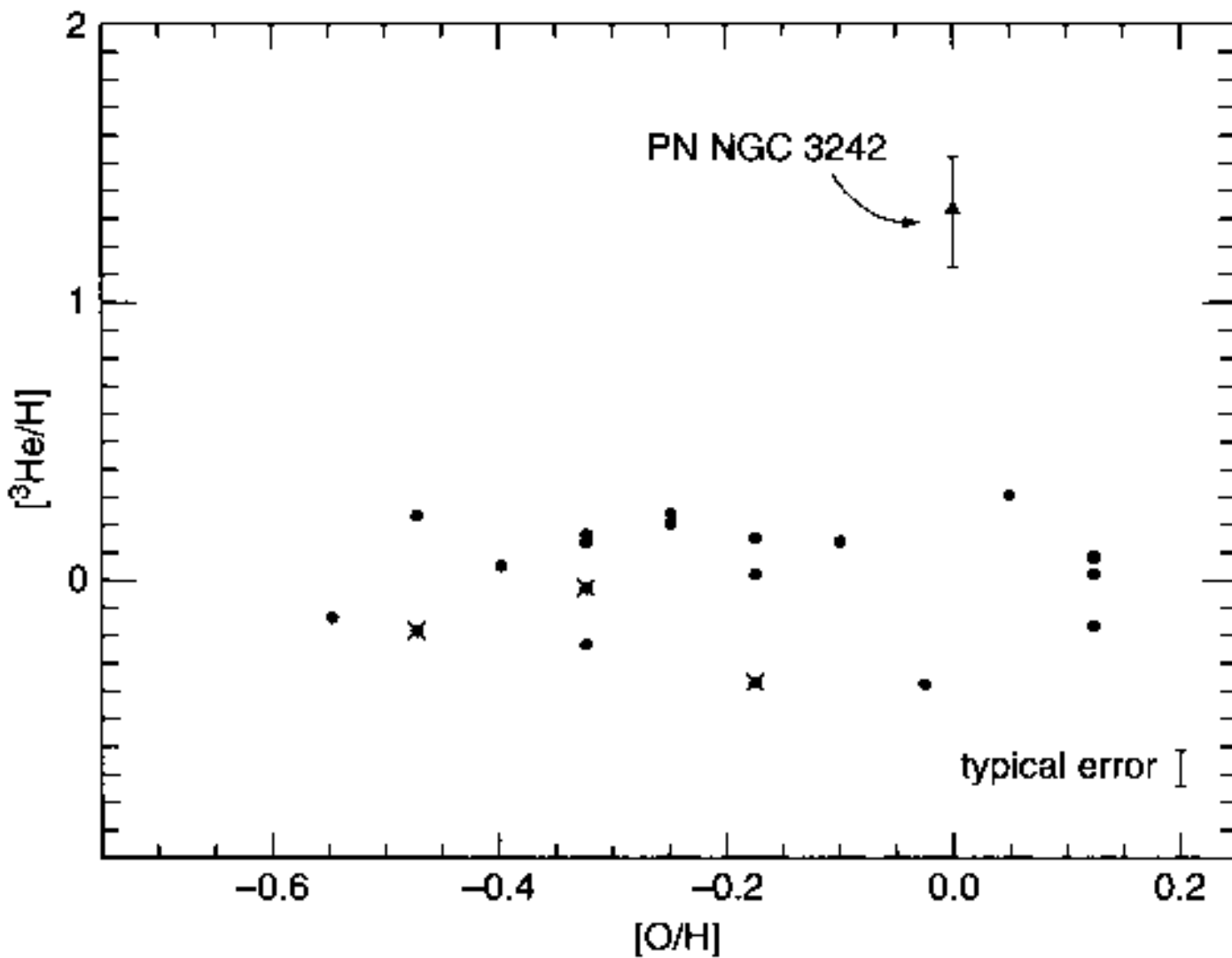


Fig. 4.7. ${}^3\text{He}/\text{H}$ in ‘simple’ Galactic H II regions, i.e. those thought to be reasonably well represented by homogeneous spherical models (Balser *et al.* 1999), and one planetary nebula, as a function of their oxygen abundance. ${}^3\text{He}/\text{H}$ is plotted on a logarithmic scale relative to the proto-solar value of 1.5×10^{-5} . After Bania, Rood and Balser (2002). Reprinted by permission from Macmillan Publishers Ltd. Courtesy Tom Bania.

Table 4.2. Interstellar and proto-solar deuterium and ^3He

	ISM	Pre-solar
$10^5 (\text{D} + ^3\text{He})/\text{H}$	3.6 ± 0.3	3.6 ± 0.35
10^5 D/H	1.5 ± 0.2	2.0 ± 0.35
$10^5 ^3\text{He/H}$	2.1 ± 0.2	1.5 ± 0.06

Data from Geiss and Gloeckler (2003).

Y_p has been measured in a variety of objects
with differing metallicities and
extrapolating to zero metallicity

$$Y = Y_p + z \frac{\Delta Y}{\Delta z} = Y_p + (O/H) \frac{\Delta Y}{\Delta (O/H)}$$

Sun is relatively young \rightarrow larger Y_p

metal-deficient stars in globular clusters
 \rightarrow born with essentially primordial
He abundance

Table 4.3. *Estimates of primordial helium mass fraction*

Objects	Y_P	Method	Ref.	Problems
Sun	$< .28 \pm .02$	Interior	1	κ ; Eq. of st.
""	$< .28 \pm .05$	Prom. He I	2	Level pops.
B stars	$< .30 \pm .04$	Abs. lines	3	Precision
μ Cas	$.23 \pm .05$	Bin. orbit	4	Precision
Globular clusters	.23: $.244 \pm .006$: $.23 \pm .02$: $\leq .24 \pm .02$	RR, Δm N(HB)/N(RG) M15 HB 47 Tuc HB	5 6 7 8	Physical basis of stellar evolution
Gal. neb.	$.22 \pm .02$.22:	Plan. neb. H II reg.	9 10	Self + gal. enr. He^0 ; gal. enr.
Extra-galactic H II regions	$.233 \pm .005$ $< .243 \pm .010$ $.228 \pm .005$ $.234 \pm .002$ $.244 \pm .002$ $.250 \pm .004$ $.249 \pm .003$ $.247 \pm .003$	Irr. + BCG BCG Irr. + BCG Irr. + BCG BCG BCG BCG + Irr. Irr. + BCG	11 12 13 14 15 16 17 18	He^0 ; data II Zw 40 I Zw 18

References: 1. Turck-Chièze & Lopez (1993). 2. Heasley & Milkey (1978). 3. Kilian (1992). 4. Haywood, Hegyi & Gudehus (1992); Drummond, Christou & Fugate (1995). 5. Caputo, Martínez Roger & Páez (1987); Sandquist (2000). 6. Buzzoni *et al.* (1983); Cassisi *et al.* (2003). 7. Dorman, Lee & VandenBerg (1991). 8. Dorman, VandenBerg & Laskarides (1989). 9. Peimbert (1983). 10. Mezger & Wink (1983). 11. Lequeux *et al.* (1979). 12. Kunth & Sargent (1983). 13. Pagel *et al.* (1992). 14. Olive, Steigman & Skillman (1997). 15. Izotov & Thuan (1998). 16. Fukugita & Kawazaki (2006). 17. Izotov, Thuan & Stasinska (2007). 18. Peimbert, Luridiana & Peimbert (2007).

most precise Y_p from recombination lines
of H & He in emission spectra of planetary
nebulas & H II regions

recent attempts to determine He abundance
in low- z H II regions

$$\Rightarrow Y = 0.2509 \pm 0.0012 + 52 \pm 9 (\%_{\text{H}})$$

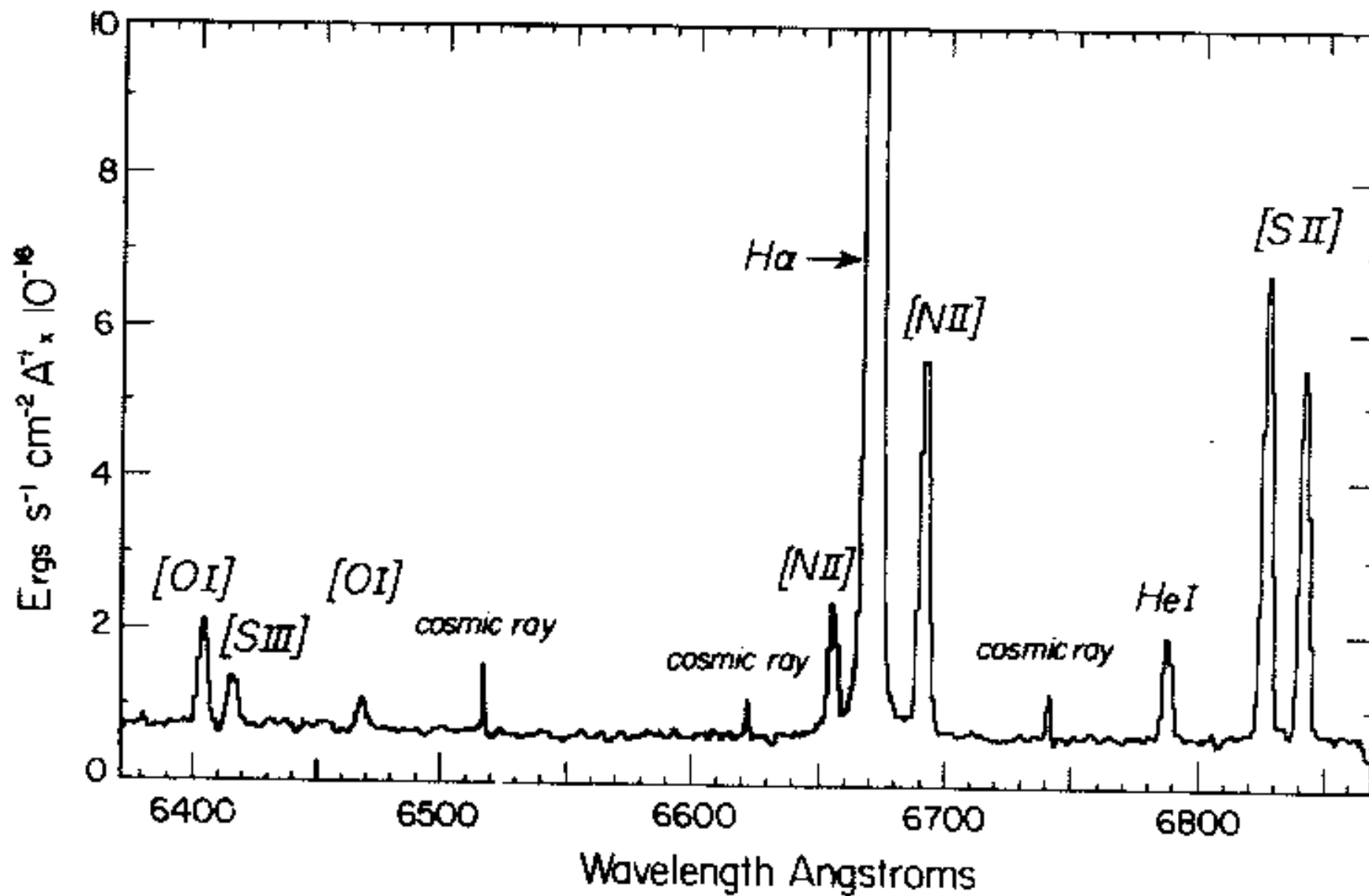


Fig. 4.10. Portion of the red spectrum of the H II galaxy Tololo 0633-415 with a redshift of 0.016, showing diagnostic features for helium ($H\alpha$ and λ 6678), electron density ([S II]) and ionization ([S III]). The features marked 'cosmic ray' are due to impacts of charged particles on the CCD detector. After Pagel *et al.* (1992).

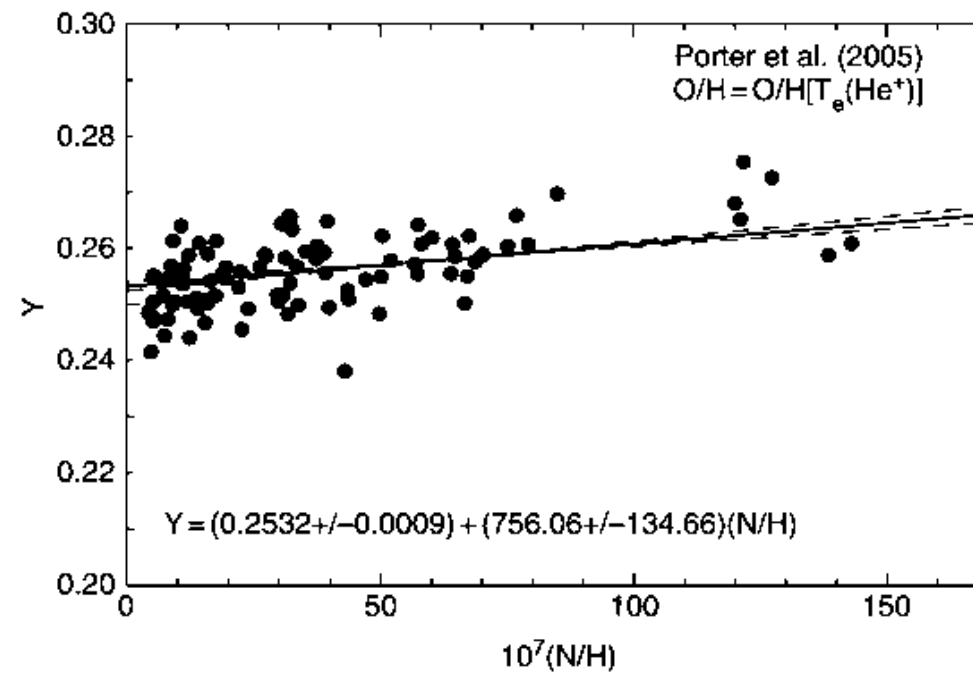
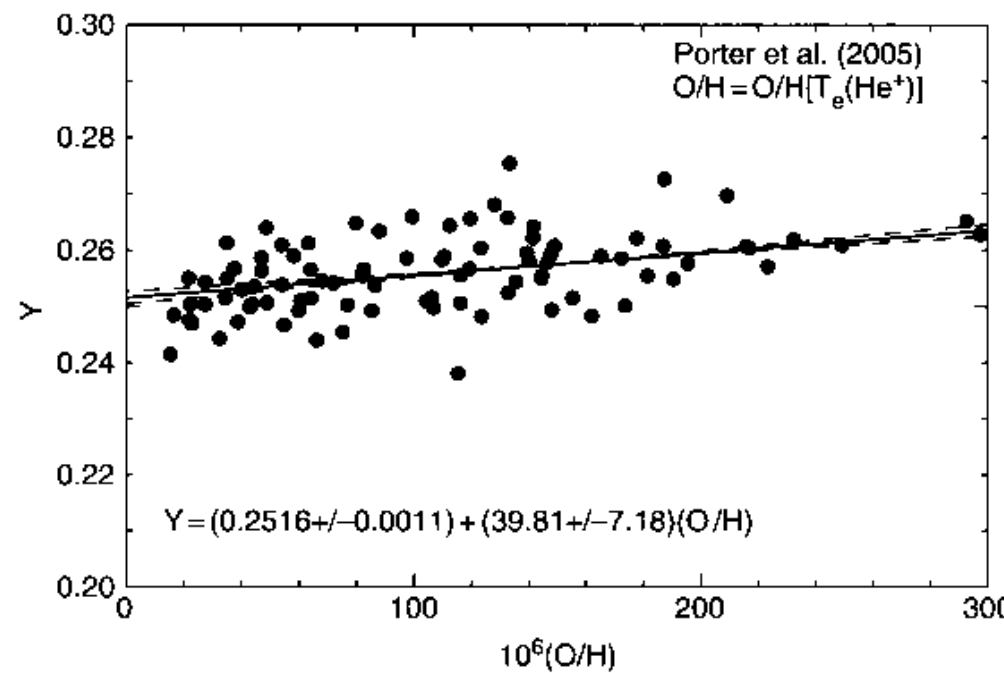


Fig. 4.11. Regressions of helium against oxygen and nitrogen in extragalactic H II regions, after Izotov, Thuan and Stasinska (2007).

Lithium ?

$$\frac{\text{Li}}{\text{H}} = 2 \cdot 10^{-9} \quad \text{derived from meteorites}$$

Li plateau for stars with $T_{\text{eff}} > 5500 \text{ K}$

extending down to $[\text{Fe}/\text{H}] \leq -4$

close to primordial abundance in Population II stars

true primordial Li abundance lower than plateau
because of nucleosynthesis in stars

$$12 + \lg (\text{Li/H}) = 2,0$$

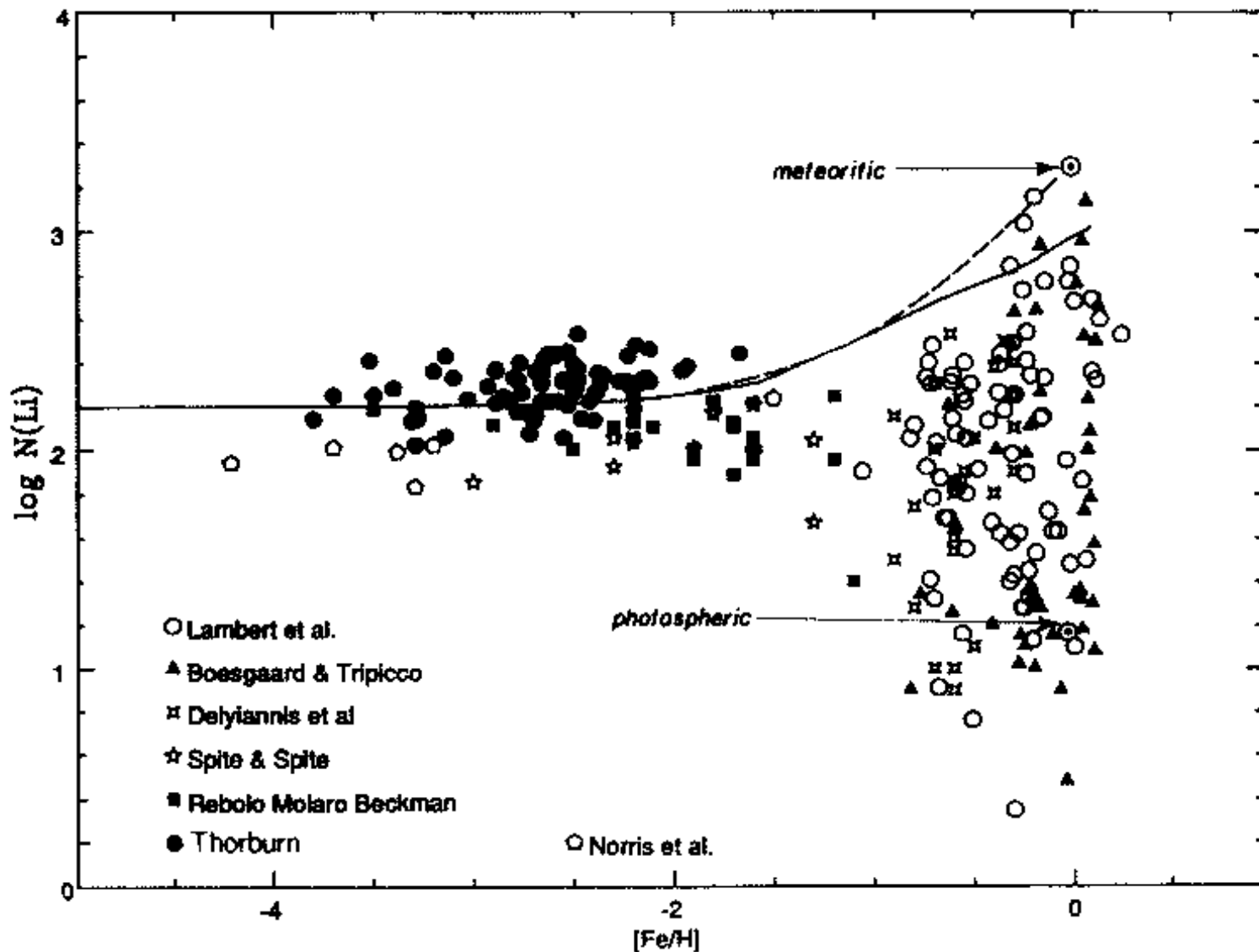


Fig. 4.12. Stellar lithium abundances (log of the number per 10^{12} H atoms) among main-sequence stars as a function of metallicity. The full-drawn curve shows the prediction of a numerical Galactic chemical evolution model, while the broken-line curve gives the sum of a primordial component and an additional component proportional to iron and normalized to meteoritic abundance. Adapted from Matteucci, D'Antona and Timmes (1995).

Small amount of ^6Li detected in stars $\sim 5\%$

^6Li not produced in BBNs \rightarrow spallation in cosmic rays

discrepancy of \sim factor 3 between

^7Li abundance on plateau extrapolation to zero metallicity & cosmological parameters

deduced from 3-15 MeV observations

currently is most serious disagreement

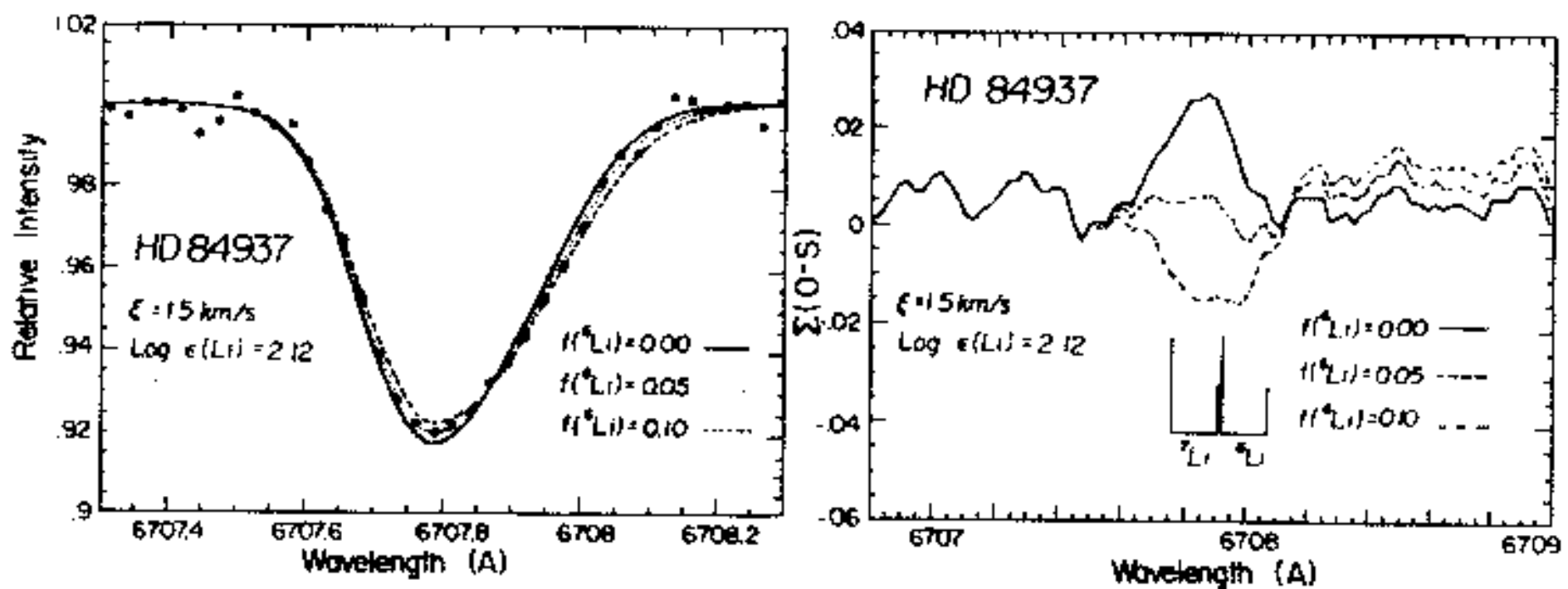


Fig. 4.13. Evidence for the presence of 5 ± 2 per cent ${}^6\text{Li}$ in the warm halo subdwarf HD 84937 with $[\text{Fe}/\text{H}] = -2.4$, $T_{\text{eff}} = 6090$ K. The left panel shows synthesized profiles for 0, 5 and 10 per cent ${}^6\text{Li}$ with the observational points on an absolute wavelength scale in the rest frame of the stellar photosphere. The right panel shows the central wavelengths of the doublets of each isotope and a deviation plot for the three hypotheses on ${}^6\text{Li}/{}^7\text{Li}$. Adapted from Smith, Lambert and Nissen (1993).

BB theory is remarkably successful

(only problem is τ_{li})

→ strong limits on baryonic density

most robust for $2 < 10^5(D/H) < 4$

$$\Rightarrow 4.5 \leq \gamma_{10} \leq 7 \quad \text{or} \quad 0.015 \leq \Omega_{bo} h^2 \leq 0.025$$

$$\text{or} \quad 0.03 \leq \Omega_{bo} \leq 0.05$$

agrees well with result of WMAP

$$\Omega_{bo} h^2 = 0.0223 \pm 0.0009$$

$$\Omega_{bo} = 4.3 \cdot 10^{-2} \pm 1.7 \cdot 10^{-3} \quad h = 0.72$$